Disruption and Formation of Arctic Staircases by Shear

Justin M. Brown[1], **Kristen Ainslie**[1], **and Timour Radko**[1]

[1]Naval Postgraduate School, Monterey, California

Key Points:

- We establish conditions for the disruption of staircases by strong vertical shear associated with internal waves
- Weak shear can lead to the formation of staircases under Arctic conditions
- Moderate isotropic shear can affect the staircase by inducing layer-merging events

Corresponding author: Justin M. Brown, `jmbrown2@nps.edu`

Abstract

Though thermohaline staircases exist in a large region of the Arctic, the interactions of such staircases with shear and turbulence are still largely unexplored. We perform a series of two- and three-dimensional simulations with and without shear and demonstrate the capacity of shear to both form and disrupt Arctic staircases. Both isotropic shear and unidirectional oscillating shear are considered. Shear is shown to disrupt staircases when the Richardson number falls below 1/4. For isotropic shear, this process works by breaking down layers individually, which leads to the gradual merging of layers, whereas the unidirectional shear tends to break down interfaces more evenly. For weaker shear (Richardson numbers greater than 2), the spontaneous development of layers is observed.

Plain Language Summary

In the Arctic, there exists a large mass of warm water below the sea ice that has origins from the Atlantic Ocean. Near the top of this layer, where the temperature decreases rapidly, there exist stacks of layers, each about 1–3m tall, within which temperature and salinity are uniform. These peculiar structures are known as "staircases," and they tend to form in regions that are deep enough that these layers are shielded from the near surface ocean turbulence. Because they exist in regions where temperature rapidly changes with depth, the heat fluxes through them could have consequences for the rate of sea-ice melt, potentially serving as a gatekeeper protecting the sea ice from the warm water of Atlantic origin. We investigate the sensitivity of these structures to wave-induced motions both in the capacity of turbulence to destroy these layers and its ability to form them.

1 Introduction

The origin and stability of thermohaline staircases remain topics of significance and mystery in studies of the Arctic Ocean. Thermohaline staircases take the form of layers of uniform temperature and salinity separated by thin interfaces with sharp gradients and typically exist in regions of the ocean of notable salt and temperature stratification. Some well-studied examples include the thermocline at mid-latitudes in the western Atlantic (Schmitt et al., 1987, 2005) and in the outflow of the Mediterranean (Tait & Howe, 1968; Magnell, 1976). The present study examines so-called diffusive staircases that are commonly observed in the Arctic. In the Eurasian Basin of the Arctic Ocean, warm water enters from the Atlantic and subducts beneath the cooler and fresher waters of the upper Arctic generating the Arctic thermocline. This is compounded by brine rejection of forming ice, which results in salty water descending along the shelf until it reaches neutral buoyancy at the halocline (see, for example, Wells & Wettlaufer, 2007; Turner, 2010). At the top of the thermocline, staircases have been observed in a number of studies, first by Neal et al. (1969) and most recently by Timmermans et al. (2008) and Shibley et al. (2017). One of the important circumstances around these staircases is that they exist between the warm water of Atlantic origin and the cooler waters above. The heat stored in the Atlantic waters is substantial, enough to melt the entirety of the Arctic sea ice (Turner, 2010); thus, it is important to understand the dynamics of this region and quantify the heat transport through it.

One of the aspects of thermohaline staircases that remains largely unknown is the nature of their interactions with turbulence and shear. Basic studies (such as that of Flanagan et al., 2013) have typically ignored the effects of shear or turbulence. A recent study by Shibley and Timmermans (2019) used a simplified model to explain the fact that staircases are observed less frequently in more turbulent environments of the Arctic, for example, locations without substantial sea-ice cover. Conversely, Radko (2016) showed that weak shear could potentially cause the development of staircases under Arctic conditions.

The impact of shear is measured in terms of the Richardson number, defined as

$$\mathrm{Ri} = \frac{N^{*2}}{\left(\frac{\partial u^*}{\partial z^*}\right)^2}, \tag{1}$$

where u^* is the lateral fluid velocity and N^* is the Brunt–Väisälä frequency. We use the superscript asterisk to distinguish the dimensional quantities used here from their non-dimensional counterparts. At very low Richardson numbers ($\mathrm{Ri} < 1/4$), the system becomes dynamically unstable to shear, and it is expected that any fine-scale interfaces will be shredded by the ensuing instability. However, shear in the Arctic tends to be much weaker (see, for example, Cole et al., 2014) at values closer to $\mathrm{Ri} = 10$. Recently, Brown and Radko (2021) showed that shear at $\mathrm{Ri} = 10$ can excite Holmboe waves at these interfaces, which distorts them appreciably. This raises the question of what the expected behavior of staircases might be in between these extremes.

We investigate how regions characteristic of the Arctic thermocline behave in the presence of shear through a series of numerical experiments. Our first set of experiments focuses on the effects of shear on pre-existing Arctic staircases, and we find that staircases appear to be remarkably resilient to shear, becoming disrupted only when $\mathrm{Ri} < 1/4$ where dynamical instabilities become dominant in the system. In addition, we investigate the development of the thermohaline–shear instability in an initially quiescent fluid and demonstrate that it can generate staircases.

The rest of this paper is arranged as follows. Section 2 discusses the governing equations and general modeling setup. Section 3 discusses the circumstances under which staircases are disrupted by shear. Section 4 discusses thermohaline staircase formation via shear instabilities. Finally, Section 5 provides conclusions and recommendations for future work.

2 Methods

We assume an incompressible, Boussinesq fluid and assert that the effects of planetary rotation are small. These assumptions are justified by the small scale of the simulation (a few meters) and the small variations in temperature and salinity over this region. The equations for a two-component fluid under these assumptions are given by (see, e.g., Baines & Gill, 1969):

$$\frac{\partial}{\partial t^*}\mathbf{u}^* + \mathbf{u}^* \cdot \nabla^* \mathbf{u}^* = -\frac{\nabla^* p^*}{\rho_0^*} - \frac{\rho^* g^*}{\rho_0^*}\mathbf{e}_z + \nu^* \nabla^{*2}\mathbf{u}^* + \mathbf{F}^*, \tag{2}$$

$$\frac{\partial}{\partial t^*}T^* + \mathbf{u}^* \cdot \nabla^* T^* + w^* \frac{\partial \overline{T}^*}{\partial z^*} = \kappa_T^* \nabla^{*2} T^*, \tag{3}$$

$$\frac{\partial}{\partial t^*}S^* + \mathbf{u}^* \cdot \nabla^* S^* + w^* \frac{\partial \overline{S}^*}{\partial z^*} = \kappa_S^* \nabla^{*2} S^*, \tag{4}$$

$$\rho^* = -\rho_0^* \left(\alpha^* \left(T^* + \overline{T}^* - T_0^*\right) - \beta^* \left(S^* + \overline{S}^* - S_0^*\right)\right) \tag{5}$$

$$\nabla^* \cdot \mathbf{u}^* = 0, \tag{6}$$

where $\mathbf{u}^*$ is the fluid velocity, p^* is the pressure anomaly with respect to hydrostatic pressure, T^* is the temperature perturbation with respect to the background field $\overline{T}^*$, S^* is the salinity concentration with respect to the background field $\overline{S}^*$, ρ^* is the density perturbation away from the constant ρ_0^*, and $\mathbf{F}^*$ is a forcing function. The quantities ρ_0^*, T_0^*, and S_0^* are reference values for density, temperature, and salinity, respectively. The symbol g^* denotes the gravitational acceleration, and $\mathbf{e}_z$ is the unit vector in the z direction, antiparallel to gravity. The gradients of the background fields, $\partial\overline{T}^*/\partial z^*$ and $\partial\overline{S}^*/\partial z^*$, are assumed uniform. We use the non-dimensionalization from Radko (2013), where the

length unit is given by

$$[l] = \left(\frac{\alpha^* g^* \frac{\partial \overline{T}^*}{\partial z^*}}{\nu^* \kappa_T^*} \right)^{-\frac{1}{4}}, \tag{7}$$

the time unit is given by $[t] = [l]^2/\kappa_T^*$, the temperature unit by $[T] = [l]\partial\overline{T}^*/\partial z^*$, the salinity by $[S] = \alpha^*[T]/\beta^*$, the pressure by $[p] = \rho_0^*[l]^2/[t]^2$, and the density unit by $[\rho] = \alpha^*\rho_0^*[T]$. This reduces Equations 2–6 to the following:

$$\frac{1}{\mathrm{Pr}}\left(\frac{\partial}{\partial t}\mathbf{u} + \mathbf{u}\cdot\nabla\mathbf{u}\right) = -\nabla p + (T-S)\,\mathbf{e}_z + \nabla^2\mathbf{u} + \mathbf{F}, \tag{8}$$

$$\frac{\partial}{\partial t}T + \mathbf{u}\cdot\nabla T = w + \nabla^2 T, \tag{9}$$

$$\frac{\partial}{\partial t}S + \mathbf{u}\cdot\nabla S = R_0 w + \tau\nabla^2 S, \tag{10}$$

$$\nabla\cdot\mathbf{u} = 0, \tag{11}$$

where $R_0 = \beta^*\frac{\partial\overline{S}^*}{\partial z^*}/\alpha^*\frac{\partial\overline{T}^*}{\partial z^*}$ is the density ratio based on the background temperature and salinity gradients, $\mathrm{Pr} = \nu^*/\kappa_T^*$ is the Prandtl number, taken to be 10 in this study, and $\tau = \kappa_S^*/\kappa_T^*$ is the inverse Lewis number. For seawater, τ is typically 0.01, but since the haline diffusivity determines required resolution of the system, it is computationally expensive to perform extended simulations at this value. Instead, we take $\tau = 0.04$ in our simulations; it has been shown (see, for example Kimura & Smyth, 2007) that changing the diffusivity ratio can have a quantitative effect on the fluxes of the system but typically does not affect qualitative behaviors.

We construct a coordinate system that moves along with a background flow, described by

$$\overline{\mathbf{u}} = \gamma(t) z\cos(\omega t)\mathbf{e}_x + \gamma'(t) z\cos(\omega t + \pi/2)\mathbf{e}_y, \tag{12}$$

where $\mathbf{e}_x$ and $\mathbf{e}_y$ are the unit vectors in the x and y directions, respectively, γ is the shear magnitude in the x direction, ω is the angular frequency of the shear oscillations, and γ' is the shear magnitude in the y direction. The temporal variability of shear consists of rapid variation in phase, associated with the oscillations of internal waves, and much slower variation in the amplitude. This study considers two distinct regimes: one which restricts the background shear to the x direction ($\gamma' = 0$), and one with isotropic shear ($\gamma' = \gamma$). The latter case is more representative of internal waves in the ocean (see, e.g., Kunze, 1990). This necessitates the following transformation to an alternate coordinate system, designated with tildes:

$$\tilde{x} = x - \frac{\gamma z}{\omega}\sin(\omega t), \tag{13}$$

$$\tilde{y} = y - \frac{\gamma' z}{\omega}\sin\left(\omega t + \frac{\pi}{2}\right), \tag{14}$$

$$\tilde{z} = z, \tag{15}$$

$$\tilde{t} = t. \tag{16}$$

We use these to transform Equations 8–11. To ensure that the background flow satisfies our expression for $\overline{\mathbf{u}}$, we require the forcing term to take the form

$$\mathbf{F} = \frac{\partial}{\partial t}\left(\gamma z\cos(\omega t)\mathbf{e}_x + \gamma' z\cos\left(\omega t + \frac{\pi}{2}\right)\mathbf{e}_y\right). \tag{17}$$

The resulting equations are solved using a modified version of the code described and used in Brown and Radko (2021). This numerical model is pseudospectral, and it decomposes the perturbation quantities with Fourier series in all three dimensions in the sheared coordinate system, and therefore, the boundaries are periodic. The code uses a modified Patterson-Orszag method to ensure incompressibility, and the time stepping is conducted with a third-order semi-implicit Adams–Bashforth/backward-differencing formula (Canuto et al., 2007; Orszag & Patterson, 1972). The nonlinear terms are calculated in physical parameter space using a three-dimensional Fourier transform.

3 Staircase Disruption

The domain for these simulations—a cube of side length $\Gamma = 200$ resolved by 384 gridpoints in each dimension—is vertically subdivided into a number of equally sized convective layers, and the total temperature, $T+\overline{T}$, and salinity, $S+\overline{S}$, within each of the layers are uniform. By construction, $\overline{T} = -z$ and $\overline{S} = -R_0 z$. These layers are separated by sharp interfaces that are initially smoothed with a boxcar filter to avoid the Gibbs phenomenon. We vary the layer height and density ratio across the simulations (see Table 1), but the size and resolution of the simulations do not vary. Each simulation has a shear angular frequency given by $\omega = N/10$, where $N^2 = \mathrm{Pr}(R_0 - 1)$ is the non-dimensional buoyancy frequency.

We gradually increase the shear strength by the domain-averaged Richardson number and observe the critical Richardson number at which the staircase is disrupted. In terms of non-dimensional quantities, the domain-averaged Richardson number is given by

$$\mathrm{Ri} = \frac{\mathrm{Pr}\,(R_0 - 1)}{\gamma^2}, \tag{18}$$

for cases with isotropic shear (i.e., $\gamma' = \gamma$). The shear magnitude, γ is chosen such that

$$\gamma(t) = \gamma_0 + \gamma_r t, \tag{19}$$

$$\gamma_0 = \sqrt{\frac{\mathrm{Pr}(R_0 - 1)}{\mathrm{Ri}_0}}, \tag{20}$$

$$\gamma_r = \sqrt{\frac{\mathrm{Pr}(R_0 - 1)}{t_\mathrm{f}}}\left(\frac{1}{\sqrt{\mathrm{Ri}_0}} - \frac{1}{\sqrt{\mathrm{Ri}_\mathrm{f}}}\right), \tag{21}$$

where $\mathrm{Ri}_0 = 1$ is the initial Richardson number of the simulation and $\mathrm{Ri}_\mathrm{f} = 0.15$ is the Richardson number at $t = t_\mathrm{f} = 100$. To determine the critical Richardson number at which staircases are disrupted, we simulate three background density ratios $R_0 = [2, 3, 5]$ with $n_\mathrm{l} = [2, 3, 4]$ starting layers, as listed in Table 1, for a total of nine simulations with isotropic shear. For comparison, we also include a simulation with $R_0 = 3$, $n_l = 3$, and unidirectional shear (i.e., $\gamma' = 0$).

The typical early state of a simulation with $\gamma' = \gamma$, $R_0 = 3$, and $n_\mathrm{l} = 3$ is shown in Figure 1a. Figure 1 depicts the non-dimensional density, defined as

$$\rho = -(T - z) + (S - R_0 z). \tag{22}$$

At the start of the simulation, temperature and salinity begin diffusing across the interfaces. Because temperature diffuses faster, this results in a convectively unstable boundary forming above and below the interface, which prompts convection. Convection is fully developed by approximately $t = 20$, which corresponds to a few convective overturning times. The mixing caused by convection results in the steepening of the interface gradients, and these two processes would typically compete until they reach an equilibrium in the absence of shear. However, convection also mixes the velocity in the convective layers, resulting in strong shear at the interfaces. As the simulation progresses, the Richardson number gradually decreases, eventually disrupting the interfaces by shearing instabilities as is shown in Figure 1b.

The evolution of the temperature fluxes is shown in Figure 2 for simulations with $R_0 = 3$, though the flux evolution is qualitatively comparable for all cases. We measure the turbulent heat flux with the domain-averaged thermal dissipation, which is given by

$$F_T = \langle(\nabla T)^2\rangle, \tag{23}$$

$$F_T^* = \rho_0^* c_p^* F_T \frac{[l]}{[t]}[T], \tag{24}$$

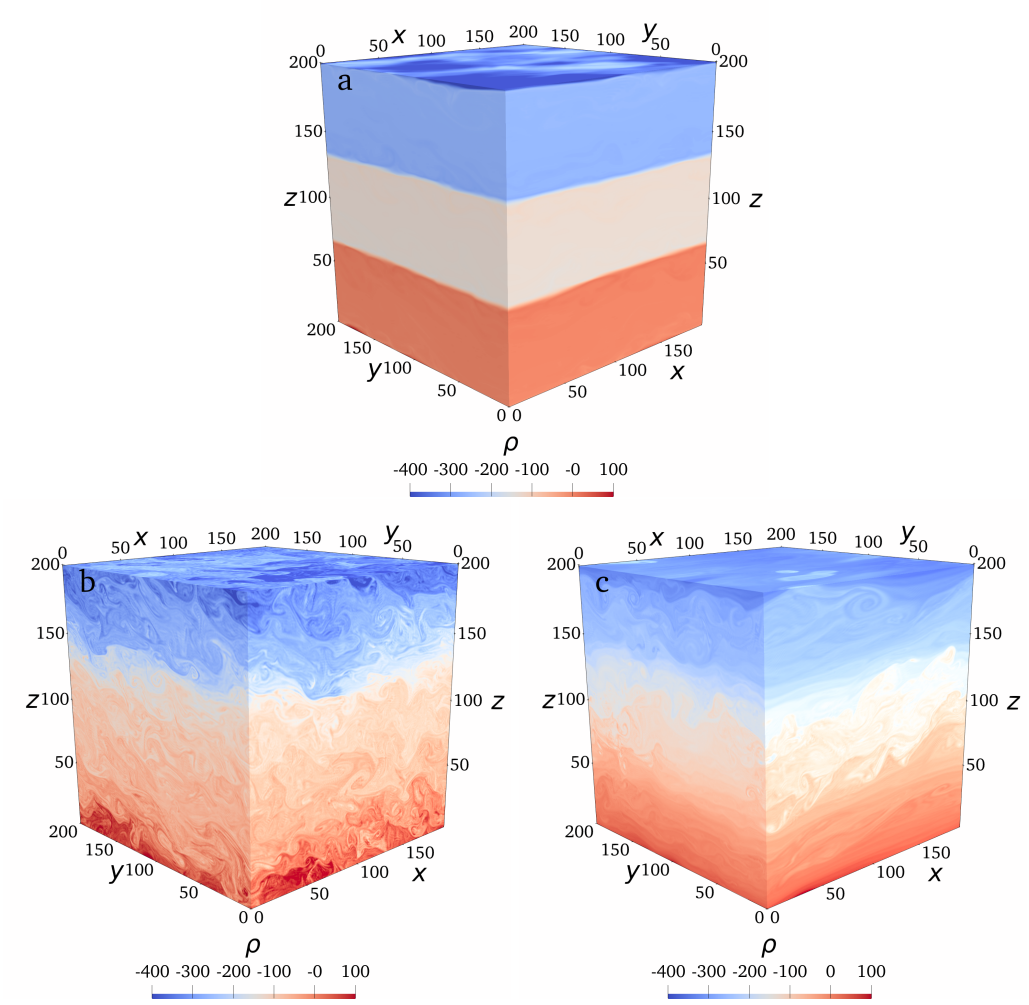

Figure 1. (a) A volume rendering of the density field in a simulation with $n_l = 3$, $R_0 = 3$, and isotropic shear at an early time, just after the simulation has begun. (b) The same rendering at a later stage, once the shear has disrupted the initial interfaces. (c) The same rendering for a unidirectional simulations with the same density ratio and number of layers.

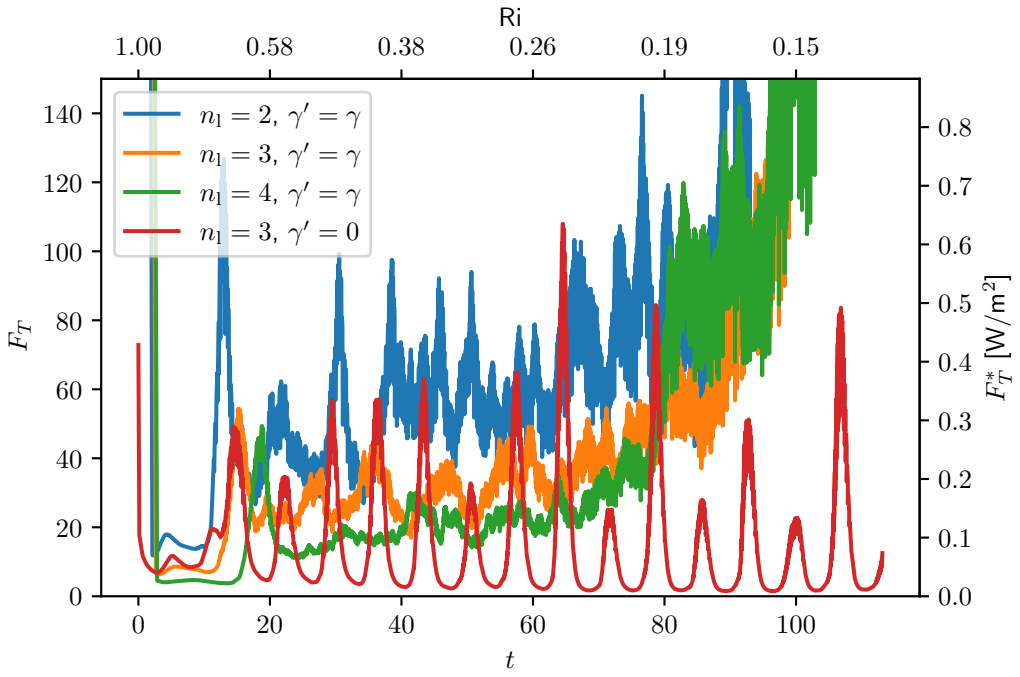

Figure 2. The evolution of the domain-averaged turbulent heat flux for simulations with $R_0 = 3$. The dimensional heat fluxes are shown on the right axis, and the Richardson number for the isotropic cases is shown on the top axis. The red curve shows the evolution of the case with unidirectional shear.

in non-dimensional and dimensional quantities, respectively. The angled brackets indicate the spatial average over the entire domain and $c_p^* = 4200\text{J/kg}^\circ\text{C}$ is the specific heat capacity of seawater. Initially, the fluxes are low prior to the onset of convection, which is fully realized by $t = 20$. After this point, the fluxes reach a temporary quasi-steady equilibrium; however, as shear continues to increase, the forced shear begins to impart energy to the convection, which is evidenced by the increasing fluxes. Eventually the flux rapidly increases due to a large mixing event in all cases, which is connected to the eventual disruption of the staircase.

Figure 2 also highlights the difference between those simulations with isotropic shear and those with unidirectional shear. It should be noted that because the shear magnitude oscillates in the unidirectional-shear simulation, the Richardson numbers given are associated with the temporal maximum of shear. Both classes of simulation begin with low heat fluxes that increase as the magnitude of the shear forcing increases. However, the unidirectional-shear simulation shows a strongly oscillatory heat flux at the shear frequency while the multidirectional-shear case does not. In addition, the peak fluxes for the unidirectional-shear case tend to be significantly higher (by about a factor of two) than in the comparable isotropic-shear case prior to the complete destruction of the interface. Though the interfaces are destroyed in all of these cases by the time that the Richardson number falls below 0.2, there is no analogous strong mixing event in the unidirectional-shear case. This may be due to the intermittency of the shear, and unlike in the case with isotropic shear (shown in Figure 1b), the unidirectional shear case only shows small localized bursts of turbulence in Figure 1c associated with the mixing peaks in Figure 2. This could have substantial implications for stochastic changes in shear direction in the ocean.

In order to determine the time at which the staircase is disrupted, we characterize the state of the simulation through the use of a "steppiness" parameter denoted as σ. This parameter is generated by constructing a histogram of the density for each time, which has a value of $h(\rho_i, t)$ for the ith density bin, such that $\sum_{i=1}^{M} h(\rho_i, t) = 1$ for all t, where M is the number of density bins (here chosen to be 400), $\rho_1 = (1-R_0)L$, and $\rho_M = 0$. Due to the periodic nature of the domain, any values of the density outside of this range can be brought inside it by adding or subtracting some multiple of $(1 - R_0)L$, which is the constant density difference between the top and bottom of the domain. This avoids mischaracterizing fluid that has crossed the vertical boundary during the simulation. A uniform gradient density field would necessarily have $h(\rho_i, t) = 1/M$ for all i. We choose to evaluate the steppiness as

$$\sigma(t) = \sum_{i=1}^{M} \begin{cases} h(\rho_i, t), \text{ if } h(\rho_i, t) > \frac{\delta}{M}, \\ 0, \text{ otherwise,} \end{cases} \tag{25}$$

where δ is a constant that was calibrated to $\delta = 1.5$ by requiring that staircase disruption occurs at $\sigma < 0.5$. This measures the fraction of the domain that is unrepresentative of a uniform density gradient in terms of the overabundance of any particular density value.

Figure 3 shows σ values for all 10 simulations grouped by density ratio. Each simulation begins with σ near 1, indicating a nearly perfectly non-uniform density distribution. As the simulation progresses, shear continues to degrade the interfaces and subsequently, σ decreases towards 0 as the fluid becomes more uniformly distributed. It is apparent that in general, systems that begin with layers of greater height are more difficult to disrupt, with those simulations with $n_l = 2$ crossing the $\sigma = 0.5$ threshold last for all density ratios. This effect is due to the relationship between step height and interface stratification for fixed density ratio—i.e., if there are fewer interfaces, the stratification of those interfaces is greater and thus, those interfaces are more difficult to disrupt. In some cases, most notably those with $n_l = 2$, the steppiness parameter begins to increase at later times, and this corresponds to layer merger events, when the shear disrupts only some of the interfaces. The steppiness of the system initially decreases as the turbulent breakdown of the interface leads to an initially heterogenous layer, but as this convective layer gradually mixes, the steppiness recovers. The layer merging process results in more robust staircases. The effect is particularly prevalent in the case of $R_0 = 5$, $n_l = 2$, where the first layer disruption happens prior to the steppiness falling below 0.5 and thus leads to a deceptively long timescale of disruption. Generally, the staircase evolution in the unidirectional shear case is analogous to those with isotropic shear, but there is no evidence of layer merging in the unidirectional shear case.

Table 1. Critical Richardson Numbers for Simulations with Isotropic Shear

R_0	$n_l = 4$	$n_l = 3$	$n_l = 2$
2 $\gamma_0 = 3.1623$, $\gamma_r = 0.05$	0.24	0.20	0.19
3 $\gamma_0 = 4.4721$, $\gamma_r = 0.0707$	0.22	0.21 ($0.24^{\dagger}$)	0.20
5 $\gamma_0 = 6.3246$, $\gamma_r = 0.1$	0.24	0.21	0.13

†Unidirectional shear simulation.

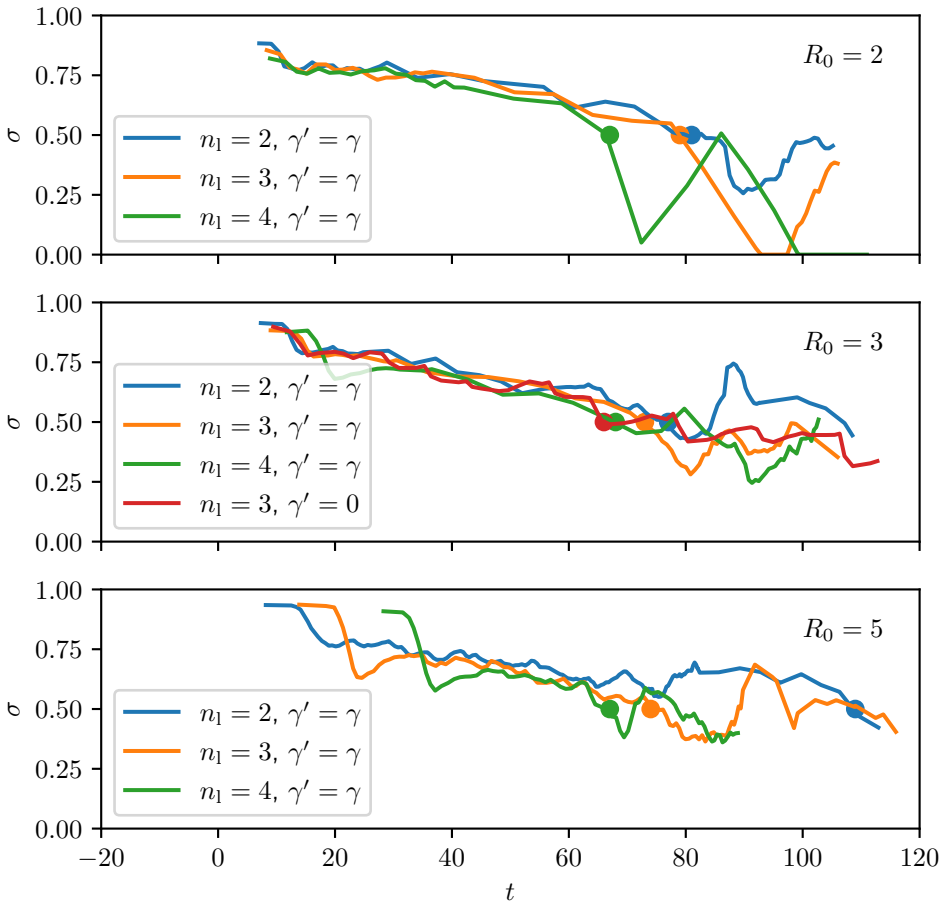

Figure 3. The evolution of the steppiness paramenter over time of simulations with (top) $R_0 = 2$, (center) $R_0 = 3$, and (bottom) $R_0 = 5$.

4 Staircase Formation

We also model staircase creation via shear instabilities through a series of two-dimensional simulations with an oceanographic value of τ. We simulated two cases with different Richardson numbers in a square box of side length $L = 100$ resolved by 3072 grid points in each dimension. Both simulations have $\mathrm{Pr} = 10$, $\tau = 0.01$, $R_0 = 2$, and $\omega = 0.3$. We characterize the simulations in terms of the mean Richardson number, given by

$$\overline{\mathrm{Ri}} = 2\frac{\mathrm{Pr}\,(R_0 - 1)}{\gamma^2}, \tag{26}$$

where the additional factor of two accounts for the temporally averaged shear magnitude squared in 2D equalling $\gamma^2/2$. For the two cases considered here, the mean Richardson numbers are $\overline{\mathrm{Ri}} = 2$ and $\overline{\mathrm{Ri}} = 3$. Each simulation begins with uniform gradients of temperature, salinity, and velocity, of which the temperature and salinity begin with small random perturbations.

Figure 4 shows a series of density perturbation snapshots of both simulations. Figures 4a,e,f show the initial development of the thermohaline—shear instability, which takes the form of exponentially growing plane waves in the sheared coordinate system, as is predicted by the linear model of Radko (2019). As these plane waves intensify, the small-scale shear in between the waves grows until the non-linear terms of the equations become important, and the system begins to develop small-scale overturns akin to Kelvin–Helmholtz instabilities, as seen in Figures 4b,g. The overturns mix the temperature and salinity locally, and the system develops into a stack of convective layers in Figures 4c,h, which is the first stage that resembles a staircase. These layers intensify over time and eventually merge to form larger layers as in Figure 4d. These systems do form layers despite being outside of the nominal range of the traditional diffusive convection instability.

The steppiness parameter is also shown for both of the staircase formation simulations in Figure 4. For these, the steppiness begins at 0, indicating a uniform density gradient. As the turbulence increases and layers begin to form, the steppiness parameter gradually increases and eventually crosses the $\sigma = 0.5$ threshold. Notably, the $\overline{\mathrm{Ri}} = 2$ simulation crosses that threshold earlier due to the higher thermohaline–shear instability growth rate for cases with lower Richardson numbers (Radko, 2019). Note that even though the number of layers in the simulation is decreasing with time (as shown in Figure 4), σ reaches a plateau at approximately 0.6. This suggests that the steppiness parameter is a relatively robust measure of the presence of a staircase and is not sensitive to the layer height in the system.

5 Discussion

Shear, isotropic or unidirectional, can have substantial impacts on the formation and disruption of themohaline staircases in the Arctic. Staircases are typically disrupted when the mean Richardson number falls below $\mathrm{Ri} = 1/4$, which is consistent with the development of dynamic instabilities at the interface. Staircases with larger layer heights are more difficult to disrupt than those with relatively thin layers. Weaker shear—Richardson numbers of 2 or more—is shown instead to have the capacity to generate layers spontaneously in a manner analogous to those of Radko (2016) and Brown and Radko (2019). The thermohaline–shear instability initially develops and amplifies, leading to the formation of layers. These layers merge in time to form large-scale staircases. We have also developed a metric to characterize staircase development in a so-called "steppiness" parameter, which uses a histogram of the density field to identify densities that are statistically overrepresented and may be interpreted as signatures of mixed layer formation.

This study supports the findings of Shibley et al. (2017) and Shibley and Timmermans (2019). Shibley et al. (2017) showed that staircases are less likely to be found in

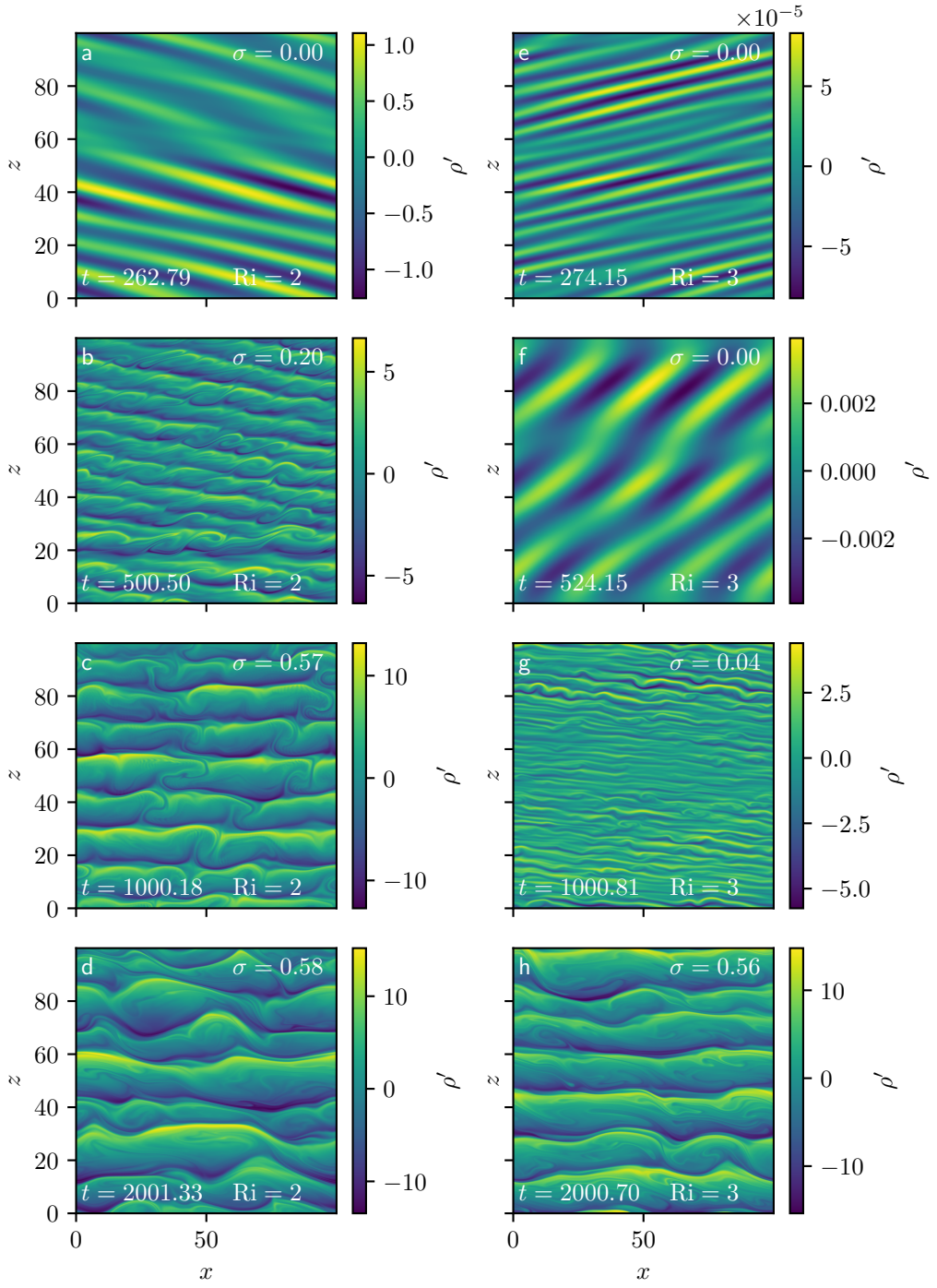

Figure 4. The density perturbations for a simulation with Ri = 2 (left) and Ri = 3 (right) developing in time from top to bottom. The steppiness of each frame is also shown.

regions where the Arctic thermocline is closer to the surface where wind forcing can lead to more turbulence. In addition, Shibley and Timmermans (2019) presented a 1-D model in which weak turbulence was shown to promote the development of convective layers, which is confirmed in our 2-D simulations. Together, these results emphasize that shear plays an important role in double-diffusive processes and that the complex interplay between these processes can have far-reaching consequences for accurately modeling the Arctic thermocline.

This research promotes a number of interesting avenues for further research. With the numerical tools that have been developed, it would be possible to find observational data of regions in the Arctic with staircases and evaluate whether these regions would develop staircases spontaneously by the thermohaline–shear instability. Conversely, it would be possible to find regions of the upper Arctic thermocline without staircases and perform numerical experiments to determine whether shear in these regions is substantial enough to disrupt any existing staircases.

Acknowledgments

Support of the National Science Foundation (grant OCE 1756491) is gratefully acknowledged. The authors acknowledge the Texas Advanced Computing Center (TACC) at The University of Texas at Austin for providing HPC resources that have contributed to the research results reported within this paper. URL: http://www.tacc.utexas.edu

Datasets produced in this study are available in Brown, Justin (2021), "Disruption and Formation of Arctic Staircases by Shear: Data from Numerical Simulations", Mendeley Data, V1, doi: 10.17632/h4pm78mdf7.1

References

Baines, P. G. G., & Gill, A. E. (1969). On thermohaline convection with linear gradients. *Journal of Fluid Mechanics*, *37*(02), 289–306. doi: 10.1017/s0022112069000553

Brown, J. M., & Radko, T. (2019). Initiation of diffusive layering by time-dependent shear. *Journal of Fluid Mechanics*, *858*, 588–608. doi: 10.1017/jfm.2018.790

Brown, J. M., & Radko, T. (2021). Diffusive Staircases in Shear: Dynamics and Heat Transport. *Journal of Physical Oceanography*, *51*(6), 1915–1928. doi: 10.1175/jpo-d-20-0193.1

Canuto, C., Quarteroni, A., Hussaini, M. Y., & Zang, T. A. (2007). *Spectral Methods.* (Spectral Model for Incompressibility in Sheared Environments SMISE) doi: 10.1007/978-3-540-30728-0

Cole, S. T., Timmermans, M.-L., Toole, J. M., Krishfield, R. A., & Thwaites, F. T. (2014). Ekman Veering, Internal Waves, and Turbulence Observed under Arctic Sea Ice. *Journal of Physical Oceanography*, *44*(5), 1306–1328. doi: 10.1175/jpo-d-12-0191.1

Flanagan, J. D., Lefler, A. S., & Radko, T. (2013). Heat transport through diffusive interfaces. *Geophysical Research Letters*, *40*(10), 2466–2470. doi: 10.1002/grl.50440

Kimura, S., & Smyth, W. (2007). Direct numerical simulation of salt sheets and turbulence in a double-diffusive shear layer. *Geophysical Research Letters*, *34*(L21610), 1–5. doi: 10.1029/2007gl031935

Kunze, E. (1990). The evolution of salt fingers in inertial wave shear. *Journal of Marine Research*, *48*(3), 471 504. doi: 10.1357/002224090784984696

Magnell, B. (1976). Salt Fingers Observed in the Mediterranean Outflow Region (34°N, 11°W) Using a Towed Sensor. *Journal of Physical Oceanography*, *6*(4), 511–523. doi: 10.1175/1520-0485(1976)006⟨0511:sfoitm⟩2.0.co;2

Neal, V. T., Neshyba, S., & Denner, W. (1969). Thermal stratification in the arctic

ocean. *Science*, *166*(3903), 373–374. doi: 10.1126/science.166.3903.373

Orszag, S. A., & Patterson, G. S. (1972). Numerical Simulation of Three-Dimensional Homogeneous Isotropic Turbulence. *Physical Review Letters*, *28*(2), 76–79. doi: 10.1103/physrevlett.28.76

Radko, T. (2013). Double-Diffusive Convection. *Double-Diffusive Convection*. doi: 10.1017/cbo9781139034173.016

Radko, T. (2016). Thermohaline layering in dynamically and diffusively stable shear flows. *Journal of Fluid Mechanics*, *805*, 147–170. doi: 10.1017/jfm.2016.547

Radko, T. (2019). Thermohaline-Shear Instability. *Geophysical Research Letters*, *46*(2), 822–832. doi: 10.1029/2018gl081009

Schmitt, R. W., Ledwell, J. R., Montgomery, E. T., Polzin, K. L., & Toole, J. M. (2005). Enhanced Diapycnal Mixing by Salt Fingers in the Thermocline of the Tropical Atlantic. *Science*, *308*(5), 685–688. doi: 10.1126/science.1108678

Schmitt, R. W., Perkins, H., Boyd, J. D., & Stalcup, M. C. (1987). C-SALT: An investigation of the thermohaline staircase in the western tropical North Atlantic. *Deep Sea Research*, *34*(10), 1655–1665. doi: 10.1016/0198-0149(87)90014-8

Shibley, N. C., & Timmermans, M.-L. (2019). The Formation of Double-Diffusive Layers in a Weakly Turbulent Environment. *Journal of Geophysical Research Oceans*, *124*(3), 1445 1458. doi: 10.1029/2018jc014625

Shibley, N. C., Timmermans, M.-L., Carpenter, J. R., & Toole, J. M. (2017). Spatial variability of the Arctic Ocean's double-diffusive staircase. *Journal of Geophysical Research Oceans*, *122*(2), 980–994. doi: 10.1002/2016jc012419

Tait, R. I., & Howe, M. R. (1968). Some observations of thermo-haline stratification in the deep ocean. *Deep Sea Research and Oceanographic Abstracts*, *15*(3), 275–280. doi: 10.1016/0011-7471(68)90005-3

Timmermans, M.-L., Toole, J., Krishfield, R., & Winsor, P. (2008). Ice-Tethered Profiler observations of the double-diffusive staircase in the Canada Basin thermocline. *Journal of Geophysical Research*, *113*(C00A02), 1–10. doi: 10.1029/2008jc004829

Turner, J. S. (2010). The Melting of Ice in the Arctic Ocean: The Influence of Double-Diffusive Transport of Heat from Below. *Journal of Physical Oceanography*, *40*(1), 249–256. doi: 10.1175/2009jpo4279.1

Wells, M. G., & Wettlaufer, J. S. (2007). The long-term circulation driven by density currents in a two-layer stratified basin. *Journal of Fluid Mechanics*, *572*(0), 37–58. doi: 10.1017/s0022112006003478